

UKAEA-CCFE-PR(21)66

Tingting Wu, Hongda He, Yueqiang Liu, L.
Li  Guoliang Xia, Lina Zhou

Effects of poloidal and parallel equilibrium flows on internal kink mode stability in tokamak plasmas

Enquiries about copyright and reproduction should in the first instance be addressed to the UKAEA Publications Officer, Culham Science Centre, Building K1/O/83 Abingdon, Oxfordshire, OX14 3DB, UK. The United Kingdom Atomic Energy Authority is the copyright holder.

The contents of this document and all other UKAEA Preprints, Reports and Conference Papers are available to view online free at scientific-publications.ukaea.uk/

Effects of poloidal and parallel equilibrium flows on internal kink mode stability in tokamak plasmas

Tingting Wu, Hongda He, Yueqiang Liu, L. Li[✉], Guoliang Xia, Lina Zhou

Effects of poloidal and parallel equilibrium flows on internal kink mode stability in tokamak plasmas

Tingting Wu¹, Hongda He², Yueqiang Liu^{3,a}, L. Li⁴, Guoliang Xia⁵, Lina Zhou⁶

¹Department of Physics, Xinzhou Teachers University, Xinzhou 034000, People's Republic of China

²Southwestern Institute of Physics, PO Box 432, Chengdu 610041, People's Republic of China

³General Atomics, PO Box 85608, San Diego, CA 92186-5608, United States of America

⁴College of Science, Donghua University, Shanghai 201620, People's Republic of China

⁵CCFE, Culham Science Centre, Abingdon, OX14 3DB, United Kingdom of Great Britain and Northern Ireland

⁶College of Science, Dalian Maritime University, Dalian 116026, China

a) Authors to whom any correspondence should be addressed.

E-mail: liuy@fusion.gat.com

Abstract

A systematic numerical investigation of the $n = 1$ (n is the toroidal mode number) internal kink mode (IKM) stability is carried out, for a conventional aspect ratio tokamak plasma in the presence of parallel equilibrium flow or its poloidal/toroidal projections. The computational results, obtained utilizing the recently updated MARS-F code [Y. Q. Liu et al., Phys. Plasmas 7, 3681 (2000)], show that a pure parallel flow provides minor influence on the internal kink instability as well as the mode frequency, being consistent with the intuitive understanding that the parallel flow mainly introduces a rotational transform along the equilibrium magnetic field line. The parallel flow shear somewhat destroys the (uniform) rotational transform, but the eventual (destabilizing) effect on the internal kink is still weak. On the other hand, a much stronger destabilization occurs by keeping only the poloidal or toroidal projection of the parallel flow. The computed mode growth rate is found to be symmetric with respect to the parallel flow direction, whilst the mode frequency is anti-symmetric. These symmetry properties are also confirmed by analytic calculations. The flow shear of the parallel flow component slightly weakens destabilization of the IKM by the poloidal or toroidal projection.

The plasma parallel viscosity is found to be strongly stabilizing to the IKM, independent of the parallel flow direction.

Keywords: internal kink mode, parallel flow, poloidal flow, toroidal flow

(Some figures may appear in colour only in the online journal)

1. Introduction

The internal kink mode (IKM) is an important magneto-hydrodynamic (MHD) instability in tokamaks. This is a kink mode arising in the plasma core region, where the value of the safety factor q falls below unity (and at sufficiently high plasma pressure). In a toroidal plasma, the mode typically has the toroidal mode number of $n=1$ and the dominant poloidal mode number of $m=1$, in terms of the radial displacement caused by the instability. Not only is the IKM itself a special and important MHD instability, other macroscopic phenomena, such as fishbone [1-5] and sawtooth activities [6-9] observed in tokamak plasmas, are also inherently related to IKM. Occurrence of fishbone can lead to energetic particle losses [10]. Sawtooth oscillations degrade fusion energy confinement in the plasma core and have the potential of triggering other MHD instabilities, such as providing seed islands to the neoclassical tearing mode [11]. Therefore, understanding the IKM stability physics is still an important issue despite many years of extensive studies. A key area of research during recent years is the effect of plasma flow on the mode stability.

It is well known that toroidal plasma rotation can significantly improve performance of the plasma by suppressing multiple MHD instabilities in tokamaks [12-17]. Analytical theory has shown that plasma toroidal flow, at velocities comparable to the sound speed, have a strong stabilizing effect on the ideal IKM [18]. On the other hand, sheared toroidal flow can also destabilize the mode [19]. So far, most of the studies have been focusing on the role of the toroidal rotation on the IKM stability in a tokamak plasma, with little attention being paid to the influence of a more generic equilibrium flow.

Poloidal flow is usually slow in a tokamak plasma due to neoclassical damping. This is why most of the past work only assumes toroidal equilibrium rotation. On the other hand, relatively fast poloidal flow sometimes does occur, for example in tokamak discharges where the internal transport barrier forms [20-22]. In fact, fast poloidal flow, being one order of magnitude faster than the neoclassical prediction, was found to also play an important role in forming the internal transport barrier itself.

On the stability side, nonlinear MHD simulations found that poloidal flow destabilizes the IKM in a low viscosity regime [23]. A similar conclusion was reached in an analytic study, based on the energy principle including the Coriolis and centrifugal forces [24]. This work expands the previous studies, based on systematic toroidal computations utilizing the MARS-F code [33] with the latest updates [25, 34]. As part of the results, our numerical study also confirms the destabilizing role played by the poloidal flow for the IKM. We note that this is qualitatively different from the stabilizing role found for the resistive wall mode [25].

This work considers the following physics effects, and their combinations, on the IKM instability: (i) the poloidal equilibrium flow, (ii) the parallel equilibrium flow, (iii) the plasma resistivity, and (iv) the plasma viscosity (more precisely the parallel viscosity). It is important to note that we do not assume an arbitrary poloidal flow in this study – we consider the poloidal projection of the parallel flow, with the latter being a consistent model satisfying the equilibrium mass conservation. Even though this consistent parallel flow has a toroidal projection (i.e. toroidal flow), we also include the toroidal flow model that is conventionally assumed for MHD stability analysis. The difference is that the latter has a toroidal angular frequency that is a function of the equilibrium magnetic flux surface (and thus will be referred to as the 1D toroidal flow), whilst the former (the toroidal projection of the parallel flow) is a 2D function of both cylindrical coordinates R and Z (in other words varying along both the plasma minor radius and the poloidal angle). We emphasize that both toroidal flow models, and their combination as well, satisfy the equilibrium mass conservation law.

The combined effects of plasma flow and viscosity on MHD instabilities have been extensively investigated in particular for the tearing mode [26-31]. For instance, it was found that plasma flow is destabilizing at weak perpendicular viscosity and stabilizing at strong perpendicular viscosity, for both tearing mode [31] and IKM [23]. In this work, we shall numerically study the effect of parallel flow, or its poloidal/toroidal projection, on the IKM stability in the presence of parallel plasma viscosity [32]. We find that the latter has a strong stabilizing effect on the IKM, but does not qualitatively change the destabilization nature of the two projections of the parallel flow.

The paper is organised as follow. Section 2 introduces the MHD model with parallel/poloidal equilibrium flow, as well as the equilibrium to be used in this study. Three different radial profiles for the parallel flow are specified. Sections 3 and 4 report computational results without and with plasma parallel viscosity, respectively. Section 5 draws conclusion.

2. Computational model with parallel flow and equilibrium model

2.1 MHD model with parallel/poloidal flow

In this work, we shall utilize the recently updated version of the MARS-F code [33] including toroidal and poloidal flows [25, 34] to study the IKM stability. A curvilinear flux coordinate system (s, χ, ϕ) is adopted in MARS-F, where $s = \psi_p^{1/2}$ is the radial coordinate, with ψ_p being the normalized equilibrium poloidal flux, χ a generic poloidal angle and ϕ the geometric toroidal angle. The equilibrium magnetic field is represented as

$$\mathbf{B} = \nabla\phi \times \nabla\psi + T(\psi)\nabla\phi,$$

where ψ is the equilibrium poloidal magnetic flux (not normalized here), and T the poloidal current flux function.

Within the single fluid approximation, a generic equilibrium flow can have both toroidal and poloidal components. A more convenient way is to introduce toroidal and parallel flows

$$\mathbf{V} = R^2 \left[\tilde{\Omega}(s) + \hat{\Omega}(s, \chi) \right] \nabla\phi + \rho^{-1}U(s)\mathbf{B}, \quad (1)$$

where R is the plasma major radius and ρ the equilibrium plasma density. $\tilde{\Omega}(s)$ denotes the conventional toroidal rotation frequency which is a function of the equilibrium magnetic flux, referred to as 1D toroidal flow in what follows. $\hat{\Omega}(s, \chi)$ is a generic toroidal rotation frequency introduced in Ref. [34], that varies in 2D poloidal plane. The role of this flow component in this study will be clarified later on. $U(s)$ is an 1D function varying along the plasma minor radius and representing plasma flow parallel to the equilibrium magnetic field line. This 1D quantity will be referred to as the parallel flow component in this work. It is important to note that, with arbitrary choice of the profiles for $\tilde{\Omega}(s)$, $\hat{\Omega}(s, \chi)$ and $U(s)$, the equilibrium flow defined in Eq. (1) always satisfies the mass conservation law $\nabla \cdot (\rho \mathbf{V}) = 0$.

The parallel flow can be projected along the toroidal and poloidal directions. Effects of toroidal and poloidal projections of the parallel flow on the IKM instability are the main topics of the present study. Following Eq. (1), the final toroidal and poloidal rotation frequencies are

$$\begin{aligned} \Omega_\phi(s, \chi) &= \mathbf{V} \cdot \nabla\phi = \tilde{\Omega}(s) + \hat{\Omega}(s, \chi) + \rho^{-1}U(s) \frac{T}{R^2}, \\ \Omega_\chi(s, \chi) &= \mathbf{V} \cdot \nabla\chi = \rho^{-1}U(s) \frac{\psi'}{J}, \end{aligned} \quad (2)$$

where J is the Jacobian associated with the curvilinear coordinates (s, χ, ϕ) . Based on the

above expression (2), we can define various choices of combinations that are of physical interests. By assuming $\tilde{\Omega}(s) = 0$ and $\hat{\Omega}(s, \chi) = -\rho^{-1}U(s)\frac{T}{R^2}$, we recover the case of pure poloidal equilibrium flow. Choosing $\tilde{\Omega}(s) = 0$ and $\hat{\Omega}(s, \chi) = 0$, we have a case with pure parallel flow. Considering $U(s) = 0$ and $\hat{\Omega}(s, \chi) = 0$, we recover the conventional 1D toroidal flow. Finally, we will also consider a case with the combination of 1D toroidal flow and parallel flow, by setting $\hat{\Omega}(s, \chi) = 0$.

Next, we introduce the perturbed MHD equations including parallel/poloidal equilibrium flow

$$\rho_1 = -\nabla \cdot (\rho \xi), \quad (3)$$

$$\begin{aligned} \rho(\tilde{\gamma} + in\Omega)\mathbf{v} = & -\nabla p + \mathbf{j} \times \mathbf{B} + \mathbf{J} \times \mathbf{b} - \rho \left[2\Omega \hat{\mathbf{Z}} \times \mathbf{v} + (\mathbf{v} \cdot \nabla \Omega) R^2 \nabla \phi \right] - R\Omega^2 \nabla \cdot (\rho \xi) \hat{\mathbf{R}} \\ & - \rho \kappa |k_{\parallel}| v_{th,i} \left[\mathbf{v} \cdot \hat{\mathbf{b}} + (\xi \cdot \nabla \mathbf{V}) \cdot \hat{\mathbf{b}} \right] \hat{\mathbf{b}} \end{aligned}, \quad (4)$$

$$\begin{aligned} & -U \nabla (\mathbf{v} \cdot \mathbf{B}) + U \mathbf{v} \times \mathbf{J} + U \mathbf{B} \times (\nabla \times \mathbf{v}) - \mathbf{B} \left[\rho \nabla (\rho^{-1}U) \cdot \mathbf{v} \right] \\ & (\tilde{\gamma} + in\Omega)\xi = \mathbf{v} + (\xi \cdot \nabla \Omega) R^2 \nabla \phi \\ & - \rho^{-1}U \nabla \times (\xi \times \mathbf{B}) + \rho^{-2}U \rho_1 \mathbf{B} + (\xi \cdot \nabla U) \rho^{-1} \mathbf{B} \end{aligned}, \quad (5)$$

$$(\tilde{\gamma} + in\Omega)\mathbf{b} = \nabla \times (\mathbf{v} \times \mathbf{B} - \eta \mathbf{j}) + (\mathbf{b} \cdot \nabla \Omega) R^2 \nabla \phi - \nabla \times (\rho^{-1}U \mathbf{b} \times \mathbf{B}), \quad (6)$$

$$p = -\xi \cdot \nabla P - \Gamma_0 P \nabla \cdot \xi, \quad (7)$$

$$\mathbf{j} = \nabla \times \mathbf{b} \quad (8)$$

where $\tilde{\gamma}$ is the (generally complex) eigenvalue of the instability, to be corrected by a Doppler shift frequency $in\Omega$ with $\Omega = \tilde{\Omega}(s) + \hat{\Omega}(s, \chi)$, and n being the toroidal mode number.

The fluid quantities ξ , \mathbf{v} , \mathbf{j} , \mathbf{b} , ρ_1 , P represent the plasma displacement, perturbed velocity, perturbed current density, perturbed magnetic field, perturbed density and perturbed pressure, respectively. The equilibrium magnetic field and current density are denoted by \mathbf{B} and \mathbf{J} , respectively. P is the total equilibrium pressure, ρ the unperturbed mass density. η is the plasma resistivity and is inversely proportional to the Lundquist number S . $\Gamma_0 = 5/3$ is the adiabatic coefficient. $\hat{\mathbf{R}}$ and $\hat{\mathbf{Z}}$ are the unit vectors along the major radius and the vertical direction, respectively, on the poloidal plane.

$\hat{\mathbf{b}} \equiv \mathbf{B}/B = \mathbf{B}/|\mathbf{B}|$ is the unit vector along the equilibrium magnetic field, $k_{\parallel} = (n - m/q)/R$ the parallel wave number, with m being the poloidal harmonic number and q the safety factor, $v_{th,i} = \sqrt{2T_i/M_i}$ the thermal ion velocity, with T_i and M_i being the thermal ion temperature and mass, respectively. κ denotes the strength of the parallel viscosity, which we will numerically vary in this study. The term associated with κ from Eq. (4) represents a parallel sound wave damping model. Physically, this term acts as a viscosity term that damps the perturbed parallel velocity of the plasma.

The above equations (3)-(8) are solved as an eigenvalue problem, in order to determine the stability of the IKM in the presence of generic equilibrium flow, for an equilibrium described below.

2.2 Equilibrium model

We consider a toroidal equilibrium with conventional aspect ratio of $R_0/a = 3$. The plasma boundary is assumed to have a circular cross section. The plasma equilibrium density is assumed to be constant across the minor radius. The radial profile of the surface averaged equilibrium toroidal current density is shown in Fig. 1(a). The equilibrium plasma pressure is specified in Fig. 1(b). The current density is normalized by $B_0/\mu_0 R_0$ and the plasma pressure by B_0^2/μ_0 . The equilibrium is self-consistently computed using the fixed boundary equilibrium solver CHEASE [34]. The resulting safety factor is reported in Fig. 1(c), which has the on-axis value of $q_0 = 0.88$ and the radial location of the $q=1$ surface at $s = \psi_p^{1/2} = 0.501$.

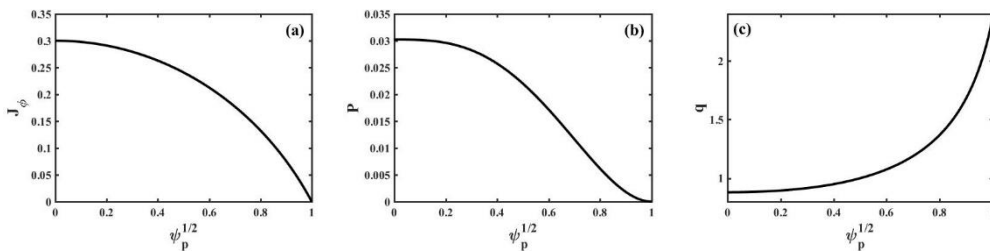


Figure 1. Radial profiles of the equilibrium quantities for (a) the flux surface averaged toroidal current density J_ϕ normalized by $B_0/\mu_0 R_0$, (b) the plasma pressure P normalized by B_0^2/μ_0 , and (c) the safety factor q with the on-axis value of $q_0 = 0.88$. Here, ψ_p is the normalized equilibrium poloidal flux.

Since the key purpose of this study is to understand the parallel/poloidal flow effect on the internal kink stability, we introduce three parallel flow profiles for $U(s)$, shown in Fig. 2. In addition to the uniform and parabolic profiles, we also consider a special profile which is constant in the plasma core and edge regions but has a strong negative flow shear near the $q=1$ surface. The radial profile for the 1D toroidal rotation frequency $\tilde{\Omega}(s)$ is always uniform in the present study. The toroidal rotation frequency is normalized by the on-axis Alfvén frequency $\omega_A = B_0/R_0\sqrt{\mu_0\rho_0}$. The parallel flow component $U(s)$ is normalized by $U_A = R_0\omega_A/B_0$. Note that in this work, the plasma flow is limited well within the subsonic range. Further on, the poloidal flow is assumed about one order of magnitude slower than the toroidal flow. That is a reasonable assumption taking into consideration the neoclassical poloidal flow damping.

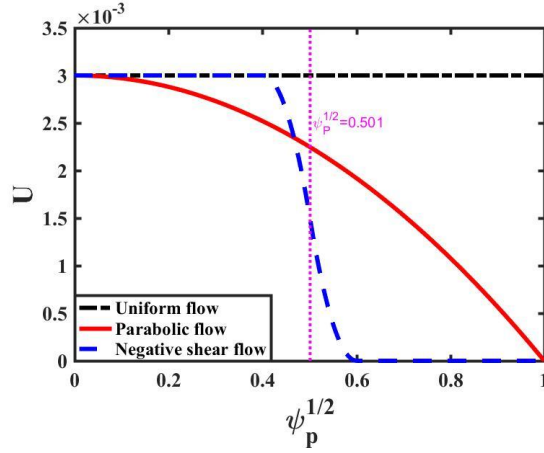


Figure 2. Three choices of the radial profile for the parallel flow component: uniform (dash-dotted line), parabolic (solid line), and step-wise constant with a local negative shear near the $q=1$ surface (dashed line). The vertical dotted line indicates the location of the $q=1$ rational surface. The parallel flow component is normalized by $U_A = R_0\omega_A/B_0$ via the on-axis toroidal Alfvén frequency

$$\omega_A = B_0/R_0\sqrt{\mu_0\rho_0}.$$

3. Computational results for ideal internal kink

In what follows, we investigate stability of the $n=1$ ideal internal kink mode, without considering finite plasma resistivity and viscosity, assuming the equilibrium and plasma flow

models described in Section 2. We shall vary the amplitude Ω_0 of the normalized (by the on-axis toroidal Alfvén frequency) 1D toroidal rotation frequency $\tilde{\Omega}(s)$ (assumed to be uniform along s) in the range from 0 to 0.05. The on-axis value of the parallel flow component $U(s)$, U_0 , will be varied within the range of -0.005 to 0.005, while maintaining the same radial profile shape for $U(s)$. Note that the same parameter U_0 will be scanned, even if only one projection (poloidal or toroidal) of the parallel flow is assumed in the stability computations. We start by considering a uniform parallel flow.

3.1. Effects of uniform parallel flow and its two projections

The MARS-F modeling finds that the uniform parallel flow generally has a very weak effect on the ideal IKM instability as shown in Fig. 3(a), where we scan both Ω_0 and U_0 . A moderate stabilization of the mode is mainly provided by the subsonic toroidal flow. At a fixed 1D toroidal flow, the counter-current parallel flow ($U_0 < 0$) is slightly destabilizing whilst the co-current parallel flow ($U_0 > 0$) is slightly stabilizing. Stabilization by the co-current parallel flow enhances with increasing toroidal flow Ω_0 . The generally weak effect of parallel flow on the IKM stability is similar to that found for other MHD modes such as the resistive wall mode [25]. An intuitive physics understanding, which is also valid for other MHD modes, is that a radially uniform parallel flow can be essentially viewed as a change of framework along the magnetic field lines. The plasma motion along the magnetic field lines therefore can hardly affect the mode stability.

The computed IKM mode frequency largely follows the 1D toroidal rotation frequency. Plotted in Fig. 3(b) is the mode frequency Doppler shifted by the toroidal rotation frequency, showing that the mode is nearly static in the plasma frame. The parallel flow has minor effect on the IKM mode frequency. There are two reasons for this. One is that the parallel flow is assumed slow compared to that of the 1D toroidal flow. The other, more interesting reason, is an almost exact cancellation for the parallel flow induced mode frequency, between the toroidal and poloidal projections, as will be demonstrated below.

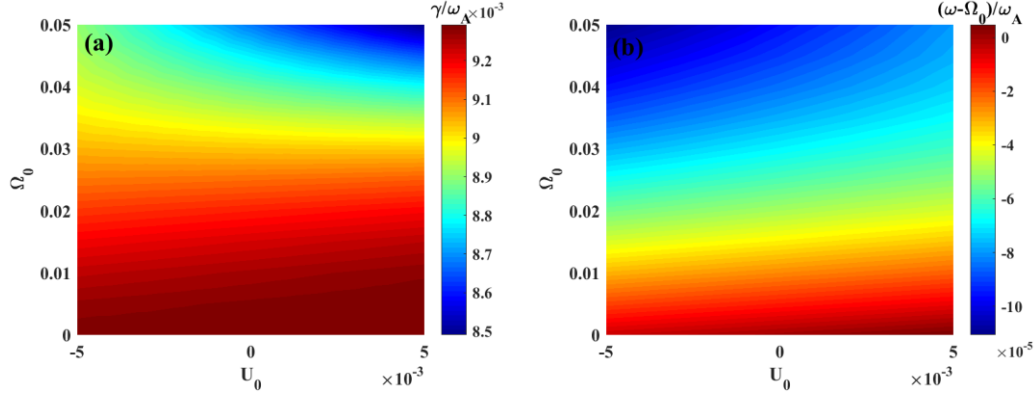


Figure 3. The MARS-F computed (a) growth rate, and (b) mode frequency Doppler-shifted by the on-axis toroidal rotation frequency, of the $n = 1$ ideal internal kink mode. Assumed is a combination of equilibrium parallel flow and 1D toroidal flow. Scanned are both the on-axis parallel flow amplitude U_0 and the on-axis toroidal rotation frequency Ω_0 . The parallel flow component is assumed uniform along the plasma minor radius.

Next, we consider effects of poloidal or toroidal projection of the parallel flow on the IKM, in combination with the 1D toroidal flow. The results are summarized in Fig. 4. The key observation is that either the poloidal or toroidal projection of the parallel flow destabilizes the IKM [Fig. 4(a,c)]. Moreover, this destabilization is independent of the direction of the parallel flow. This is different from the parallel flow results shown in Fig. 3(a), where the counter-current flow is destabilizing whilst the co-current flow is stabilizing. This symmetry in the enhancement of the IKM instability, with respect to the parallel flow direction, can be analytically understood for either the poloidal projection [24] or the toroidal projection (Appendix). The symmetry is slightly destroyed by fast 1D toroidal rotation. On the other hand, the stabilizing effect, provided by the 1D toroidal flow, is much weaker than the destabilizing effect due to either projection of the parallel flow. This is despite the fact that the 1D toroidal flow is one order of magnitude faster than the two projections of the parallel flow.

The Doppler-shifted (due to 1D toroidal rotation) mode frequency is much larger with either projection of the parallel flow [Fig. 4(b,d)], compared to that with the parallel flow [Fig. 3(b)]. Note also that (i) the Doppler shifted mode frequency is anti-symmetric with respect to the sign of U_0 , with either poloidal [Fig. 4(b)] or toroidal [Fig. 4(d)] projection; and (ii) the Doppler shifted mode frequency has opposite sign but nearly the same amplitude, between poloidal and toroidal projections. When both projections are included, i.e., with the parallel flow, cancellation occurs for the mode frequencies shown in Fig. 4(b) and (d), resulting in nearly vanishing frequency as shown in Fig. 3(b).

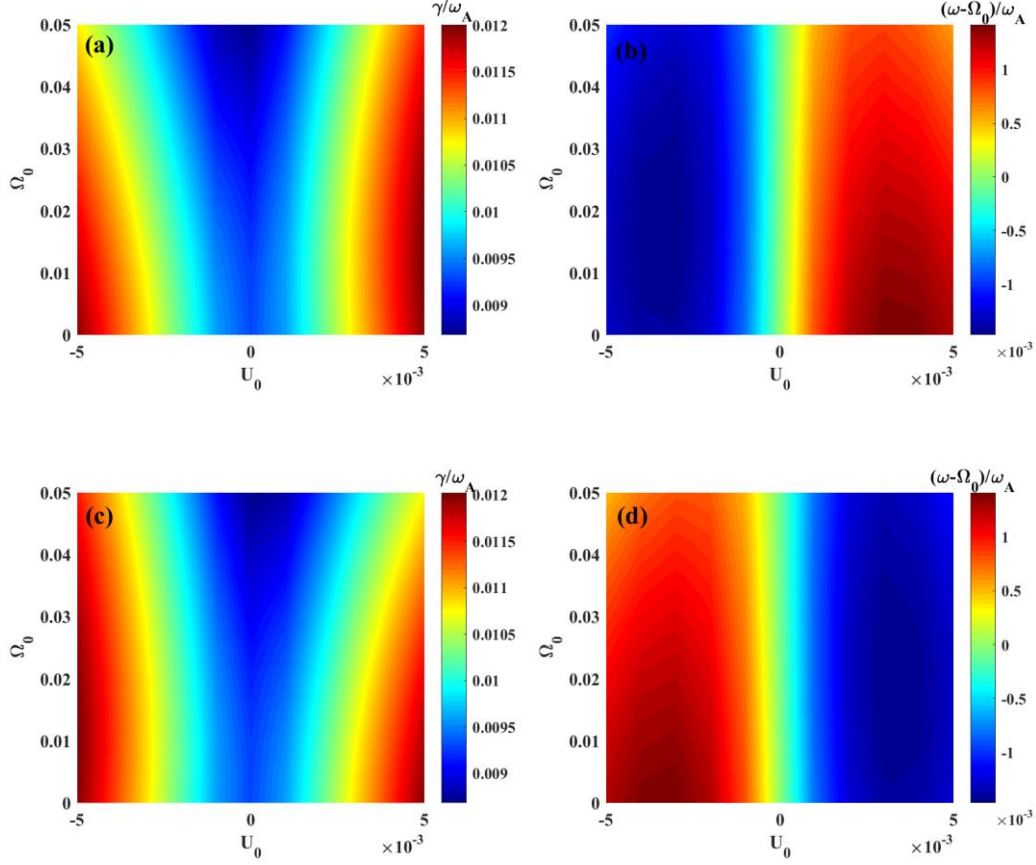


Figure 4. The MARS-F computed (a,c) growth rate, and (b,d) mode frequency Doppler-shifted by the on-axis toroidal rotation frequency, of the $n = 1$ ideal internal kink mode. Scanned are both the on-axis parallel flow amplitude U_0 and the on-axis toroidal rotation frequency Ω_0 . Assumed in (a-b) is the combination of the poloidal projection of the equilibrium parallel flow and the 1D toroidal flow. Assumed in (c-d) is the combination of the toroidal projection of the equilibrium parallel flow and the 1D toroidal flow. The parallel flow component is uniform along the plasma minor radius.

The MARS-F computed $n = 1$ ideal IKM eigenmode structure is almost identical between the two cases, with inclusion of either the poloidal [Fig. 5(a)] or toroidal [Fig. 5(b)] projection of the parallel flow. These radial profiles of poloidal Fourier harmonics of the plasma radial displacement show typical IKM eigenmode structure in a toroidal plasma: (i) the $m = 1$ harmonic is dominant over other harmonics; (ii) the $m = 1$ radial displacement remains nearly constant inside the $q = 1$ surface and quickly vanishes outside the same surface. The fact that the computed mode eigenfunction is not much modified by the (subsonic) toroidal and poloidal flows supports assumptions made in analytic calculations based on the IKM energy principle.

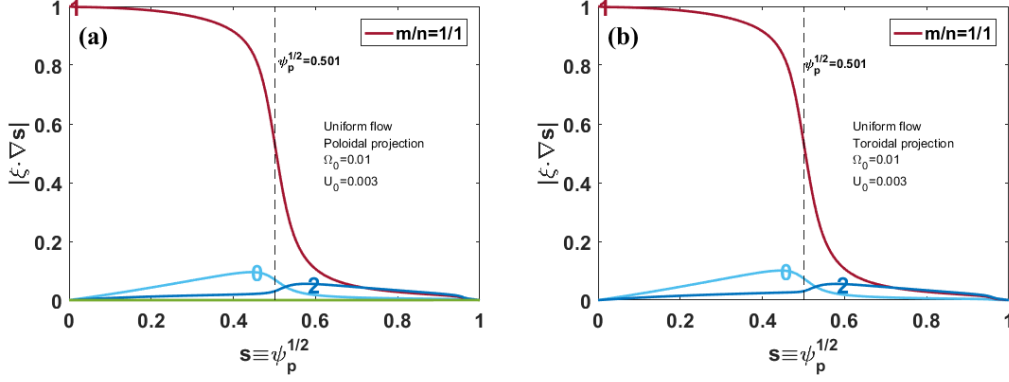


Figure 5. The eigenmode structure of the $n = 1$ ideal internal kink mode, plotted in terms of the poloidal Fourier harmonics of the plasma radial displacement and computed assuming (a) the poloidal projection, and (b) the toroidal projection, of the parallel flow with $U_0 = 0.003$. The parallel flow component is uniform along the plasma minor radius. Assumed is also finite 1D toroidal flow with $\Omega_0 = 0.01$. The vertical dashed lines indicate the radial location of the $q = 1$ surface. Shown are only three dominant Fourier harmonics although the toroidal computations includes seventeen harmonics.

3.2. Effects of parallel flow with parabolic radial profile and its two projections

Similar to subsection 3.1, we compute the IKM eigenvalue while scanning both U_0 and Ω_0 in 2D parameter space, but this time assuming a parabolic parallel flow profile as shown in Fig. 2 (red curve). Figure 6(a) shows that the parallel flow effect on the ideal IKM is still weak. But different from the case with uniform parallel flow [Fig. 3(a)], the co-current parallel flow now slightly destabilizes the mode whilst the counter-current flow offers stabilization. This shows that the (global) shear of the parallel flow also changes the IKM instability, although the effect is generally weak. Negative flow shear of the co-current parallel flow is slightly destabilizing to the ideal IKM. The Doppler-shifted mode frequency is again very small [Fig. 6(b)], indicating certain cancellation which indeed occurs as shown in Fig. 7.

Figure 7 reports the effects of poloidal [Fig. 7(a-b)] and toroidal [Fig. 7(c-d)] projections of the parabolic parallel flow on the IKM. The results are similar to that shown in Fig. 4 assuming uniform parallel flow profile, i.e., (i) either projection of the parallel flow destabilizes the IKM independent of the sign of U_0 ; (ii) the Doppler-shifted mode frequency is anti-symmetric with respect to the sign of U_0 and is opposite between the poloidal and toroidal projections, which the latter providing cancellation for the mode frequency when the parallel flow is included [Fig. 6(b)].

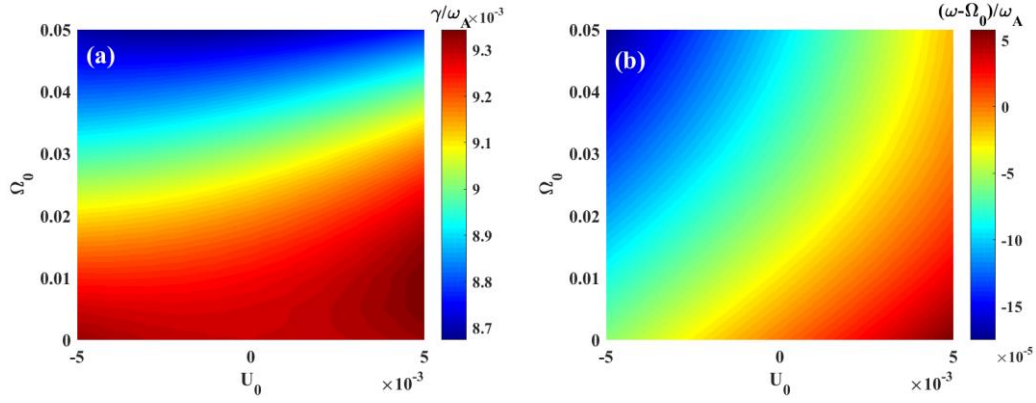


Figure 6. The MARS-F computed (a) growth rate, and (b) mode frequency Doppler-shifted by the on-axis toroidal rotation frequency, of the $n = 1$ ideal internal kin mode. Assumed is a combination of the equilibrium parallel flow and 1D toroidal flow. Scanned are both the on-axis parallel flow amplitude U_0 and the on-axis toroidal rotation frequency Ω_0 . The parallel flow component is parabolic along the plasma minor radius.

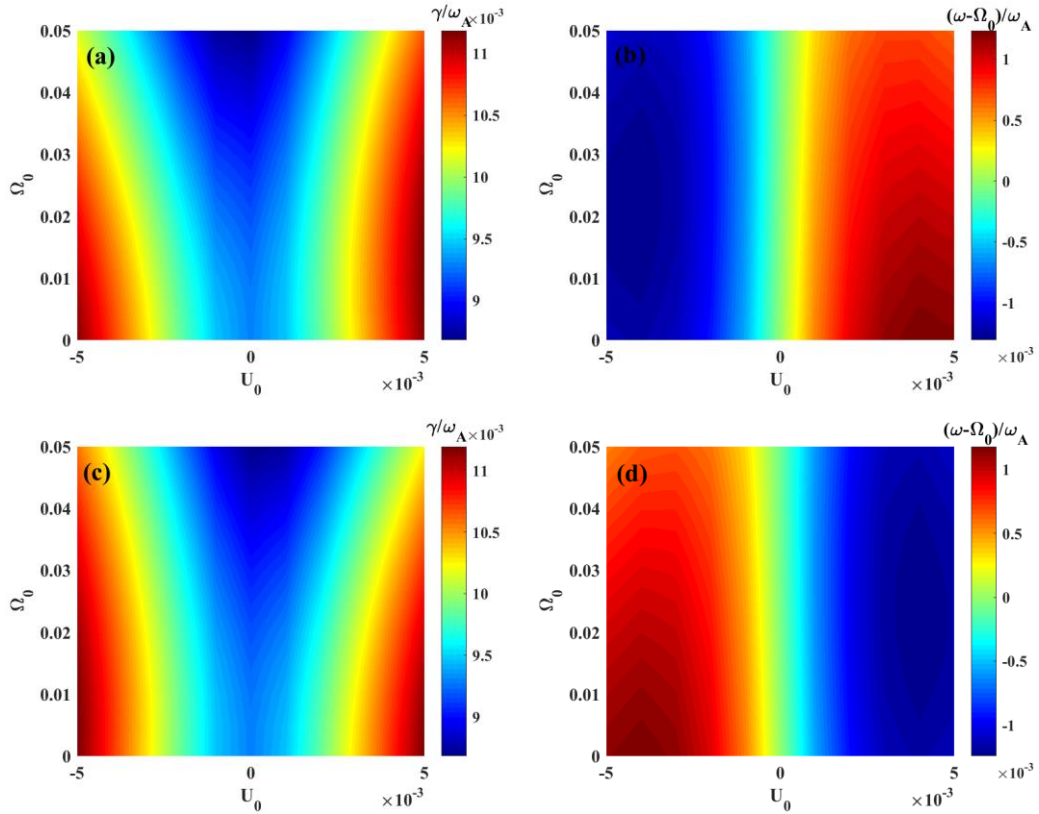


Figure 7. The MARS-F computed (a,c) growth rate, and (b,d) mode frequency Doppler-shifted by the on-axis toroidal rotation frequency, of the $n = 1$ ideal internal kink mode. Scanned are both the on-axis parallel flow amplitude U_0 and the on-axis toroidal rotation frequency Ω_0 . Assumed in (a-b) is the

combination of the poloidal projection of the equilibrium parallel flow and the 1D toroidal flow. Assumed in (c-d) is the combination of the toroidal projection of the equilibrium parallel flow and the 1D toroidal flow. The parallel flow component is parabolic along the plasma minor radius.

3.3. Effects of parallel flow with local flow shear and its two projections

Assuming a parallel flow with a locally large shear near the $q = 1$ surface (dashed blue curve in Fig. 2), MARS-F computations find qualitatively similar results for the ideal IKM stability, to that reported in subsections 3.1-2. But there are also differences as reported in Figs. 8-9. In particular, locally larger flow shear near the $q = 1$ surface of the co-current parallel flow provides stronger destabilization to the mode [Fig. 8(a)]. This destabilization mechanism is likely similar to that due to the (local) toroidal flow shear [19]. The Doppler-shifted mode frequency [Fig. 8(b)] is still small but larger than that with uniform or parabolic parallel flow, indicating less cancellation between the two projections of the parallel flow.

Indeed, assuming either projection of the parallel flow with local shear, the symmetry with respect to the sign of U_0 is less conserved, for both the computed mode growth rate [Fig. 9(a,c)] and mode frequency [Fig. 9(b,d)]. The asymmetry in the mode growth rate is largely due to the fact that the relative (stabilizing) role of the 1D toroidal flow now becomes larger. The asymmetry in the Doppler-shifted mode frequency implies less cancellation for the mode frequency induced by the poloidal and toroidal projections.

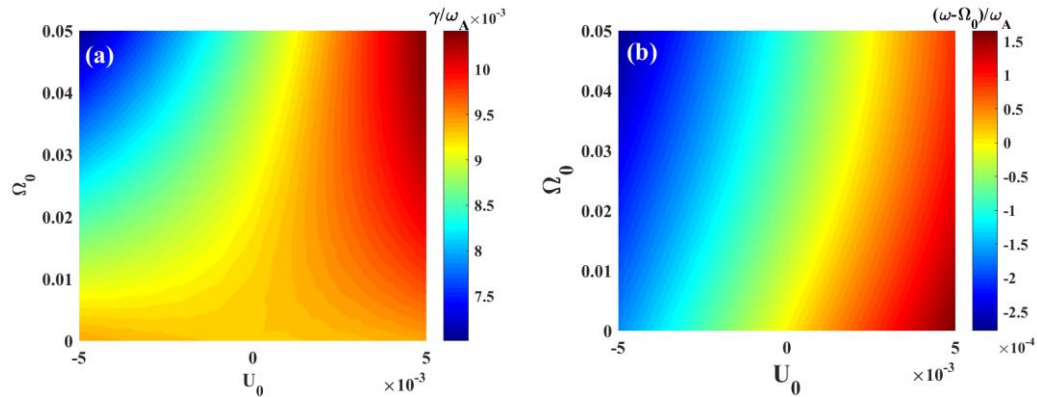


Figure 8. The MARS-F computed (a) growth rate, and (b) mode frequency Doppler-shifted by the on-axis toroidal rotation frequency, of the $n = 1$ ideal internal kink mode. Assumed is a combination of the equilibrium parallel flow and 1D toroidal flow. Scanned are both the on-axis parallel flow amplitude U_0 and the on-axis toroidal rotation frequency Ω_0 . The parallel flow component is a step-wise constant with

a local negative shear near the $q=1$ surface.

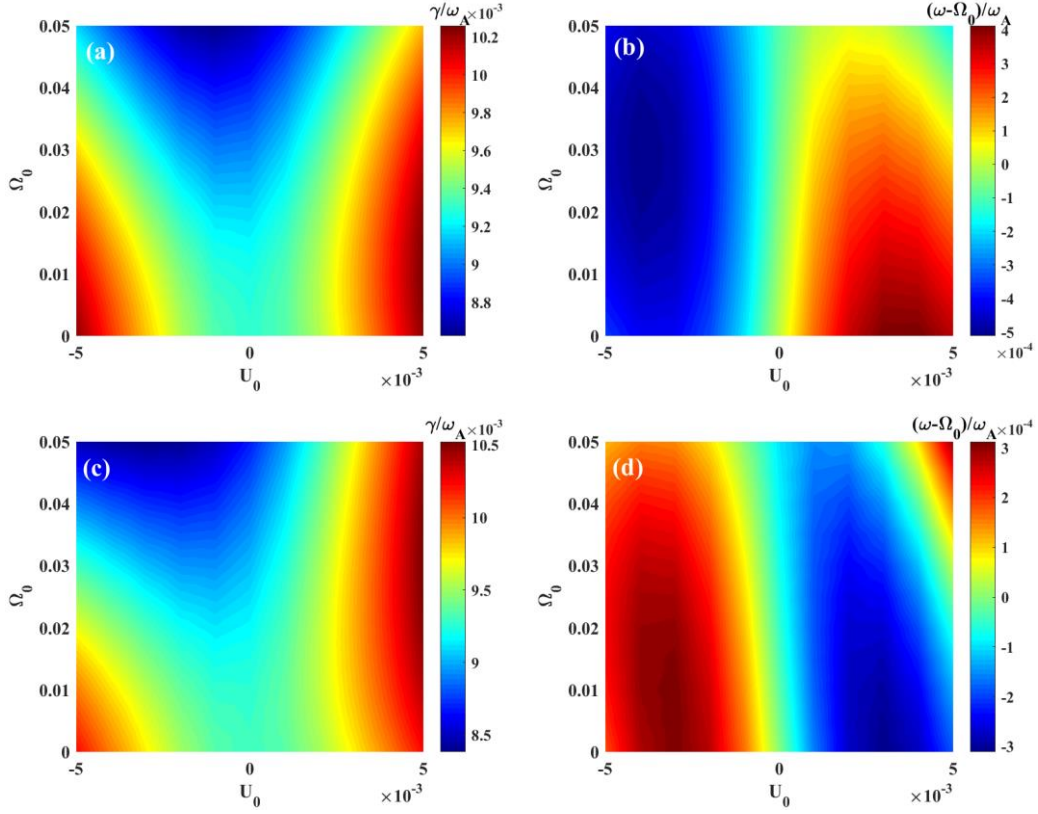


Figure 9. The MARS-F computed (a,c) growth rate, and (b,d) mode frequency Doppler-shifted by the on-axis toroidal rotation frequency, of the $n=1$ ideal internal kink mode. Scanned are both the on-axis parallel flow amplitude U_0 and the on-axis toroidal rotation frequency Ω_0 . Assumed in (a-b) is the combination of the poloidal projection of the equilibrium parallel flow and the 1D toroidal flow. Assumed in (c-d) is the combination of the toroidal projection of the equilibrium parallel flow and the 1D toroidal flow. The parallel flow component is a step-wise constant with a local negative shear near the $q=1$ surface.

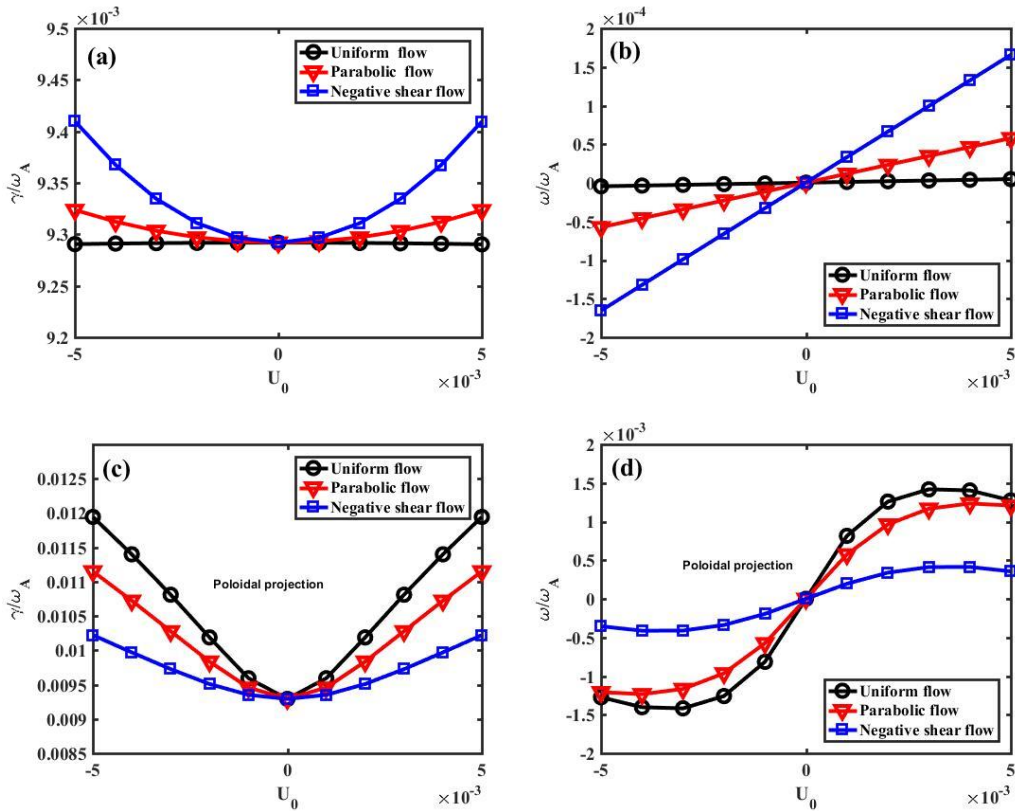
3.4. Effects of flow shear

Figure 10 compares the MARS-F computed $n=1$ ideal IKM eigenvalue, assuming three different radial profiles for the parallel flow component $U(s)$ as shown in Fig. 2. The 1D toroidal flow is excluded ($\Omega_0=0$). We thus show the effects of a pure parallel flow [Fig. 10(a-b)], or its poloidal [Fig. 10(c-d)] or toroidal [Fig. 10(e-f)] projection, on the mode stability. The overall observation is the perfect symmetry of the mode growth, and anti-symmetry of the mode frequency, with respect to the sign of U_0 . As mentioned before, this perfect symmetry

(anti-symmetry) can be analytically demonstrated for a cylindrical plasma (Ref. [24] and Appendix). But MARS-F results show that this holds also for toroidal plasmas.

In terms of quantitative comparison, we find that a pure parallel flow, with or without shear, provides very weak (destabilizing) effect to the IKM, as compared to that by the poloidal or toroidal projection of the parallel flow. A uniform parallel flow provides almost no change to the IKM eigenvalue [Fig. 10(a-b)], supporting our hypothesis that a uniform parallel flow merely yields a shift of reference frame along magnetic field lines. The flow shear of the pure parallel flow enhances the mode destabilization (as well as the mode frequency).

On the other hand, the flow shear in the parallel component $U(s)$ reduces the mode destabilization, when only the poloidal [Fig. 10(c)] or toroidal [Fig. 10(e)] projection is included into the stability calculations. This somewhat counter-intuitive result is probably related to the fact that the flow shear in the parallel component does not necessarily reflect the flow shear in its projection along the poloidal or toroidal angle. Finally, we note that the mode frequencies induced by either projection are about one order of magnitude larger than that due to the pure parallel flow, and are opposite in sign between the poloidal [Fig. 10(d)] and toroidal [Fig. 10(f)] projections.



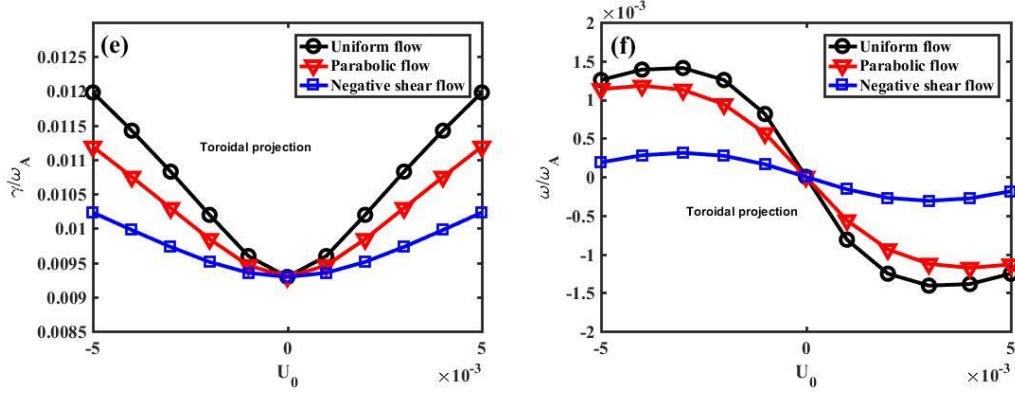


Figure 10. The MARS-F computed (a, c, e) growth rate, and (b, d, f) mode frequency, of the $n = 1$ ideal internal kink mode versus the on-axis parallel flow component U_0 , assuming three sets of parallel flow profiles shown in Fig. 2. Compared are also cases with (a,b) parallel flow, (c,d) only poloidal projection of the parallel flow, and (e,f) only toroidal projection of the parallel flow. The 1D equilibrium toroidal flow is excluded.

4. Internal kink stability with non-ideal effects

We consider two non-ideal effects in the present study: (i) the plasma resistivity and (ii) the plasma parallel viscosity. As discussed before, the parallel viscosity is modeled via a parallel sound wave damping term. We will focus on the combined effects of these non-ideal physics and a pure parallel flow (or its projections) on the IKM stability. The 1D toroidal flow will be ignored, since its combination with non-ideal effects have previously been studied, e.g., in Ref. [19].

We start by considering the aforementioned non-ideal effects on the $n = 1$ IKM instability in the absence of any equilibrium flow. Figure 11 reports the computed mode growth rate with varying viscosity coefficient κ , assuming different values of Lundquist number S . Note that the case of $S = \textit{infinity}$ corresponds to an ideal plasma (with vanishing plasma resistivity). The typical value of κ for large viscosity is of order unity within the MARS-F normalization. We find a strong stabilization of the IKM with parallel viscosity, in both ideal and resistive plasmas. The plasma resistivity, on the other hand, destabilizes the mode as is well known [4]. The eventual IKM instability is thus a result of the two competing effects from the plasma resistivity and parallel viscosity.

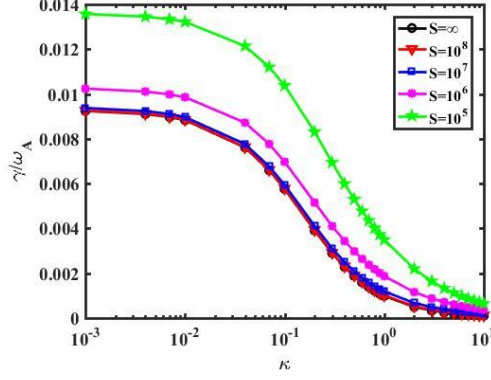


Figure 11. The MARS-F computed growth rate of the $n = 1$ internal kink mode versus the parallel viscous damping coefficient κ , with varying Lundquist number S . All equilibrium flow components are excluded.

Figure 12 reports the MARS-F computed non-ideal IKM eigenvalues in the presence of pure parallel flow. Assumed are three radial profiles for the parallel flow component $U(s)$ as shown in Fig. 2. We fix the plasma resistivity (with $S = 10^6$) and choose three representative values for the plasma viscosity: $\kappa = 0.1$ (small viscosity), $\kappa = 1$ (large viscosity), and $\kappa = 10$ (unrealistically large viscosity). The plasma parallel flow, as well as the flow shear, has negligible effect on the growth rate of the non-ideal IKM. The parallel flow effect on the mode frequency is somewhat stronger but is still moderate. These results resemble that of the ideal IKM reported in section 3.

On the contrary, the effect of the poloidal and toroidal projections of the parallel flow is much stronger on the non-ideal IKM. This is reported in Fig. 13-15, assuming three radial profiles, respectively, for the parallel flow. Similar to the case for the ideal IKM, both poloidal and toroidal projections of the parallel flow destabilize the non-ideal IKM. Note that the symmetry (anti-symmetry) of the mode growth rate (mode frequency) with respect to the sign of U_0 is also largely conserved. On the other hand, the overall strong stabilization still comes from the parallel viscosity, at large values of the viscosity coefficient.

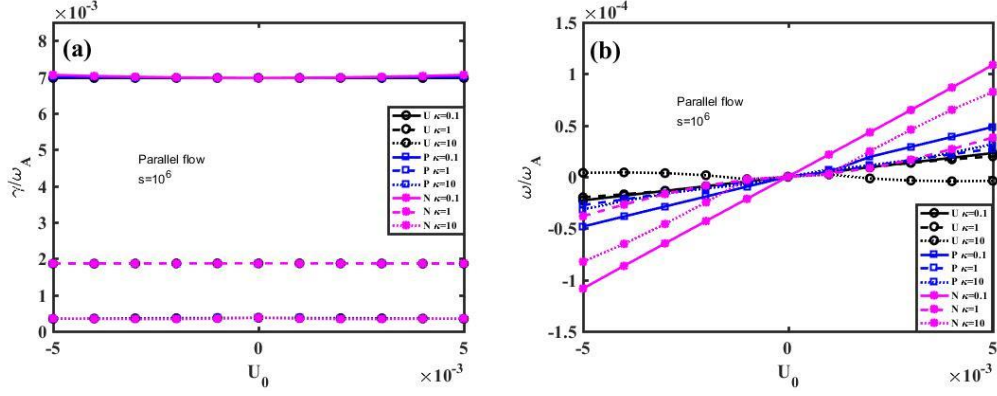


Figure 12. The MARS-F computed (a) growth rate, and (b) mode frequency, of the $n = 1$ resistive internal kink mode versus the on-axis parallel flow component U_0 , with different parallel viscous damping coefficients: $\kappa = 0.1$ (solid line), $\kappa = 1$ (dashed line) and $\kappa = 10$ (dotted line), assuming three sets of parallel flow profiles as shown in Fig. 2: uniform profile (circles), parabolic profile (squares), step-wise constant with local negative shear (stars). The Lundquist number is $S = 10^6$. The 1D equilibrium toroidal flow is excluded.

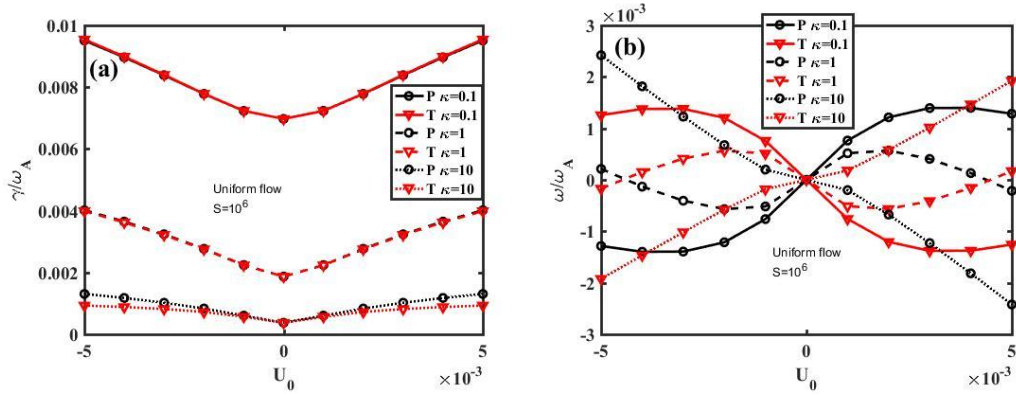


Figure 13. The MARS-F computed (a) growth rate, and (b) mode frequency, of the $n = 1$ resistive internal kink mode versus the on-axis parallel flow component U_0 , assuming poloidal projection (circles, also labeled as “P”) and toroidal projection (triangles, also labeled as “T”) of the parallel flow with different parallel viscous damping coefficients: $\kappa = 0.1$ (solid line), $\kappa = 1$ (dashed line) and $\kappa = 10$ (dotted line). The parallel flow profile is uniform. The Lundquist number is $S = 10^6$. The 1D equilibrium toroidal flow is excluded.

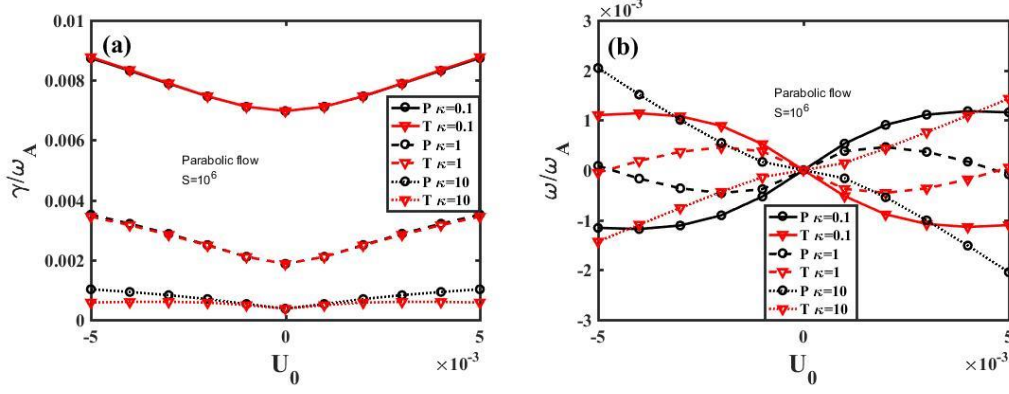


Figure 14. The MARS-F computed (a) growth rate, and (b) mode frequency, of the $n = 1$ resistive internal kink mode versus the on-axis parallel flow component U_0 , assuming poloidal projection (circles) and toroidal projection (triangles) of the parallel flow with different parallel viscous damping coefficients: $\kappa = 0.1$ (solid line), $\kappa = 1$ (dashed line) and $\kappa = 10$ (dotted line). The parallel flow profile is parabolic. The Lundquist number is $S = 10^6$. The 1D equilibrium toroidal flow is excluded.

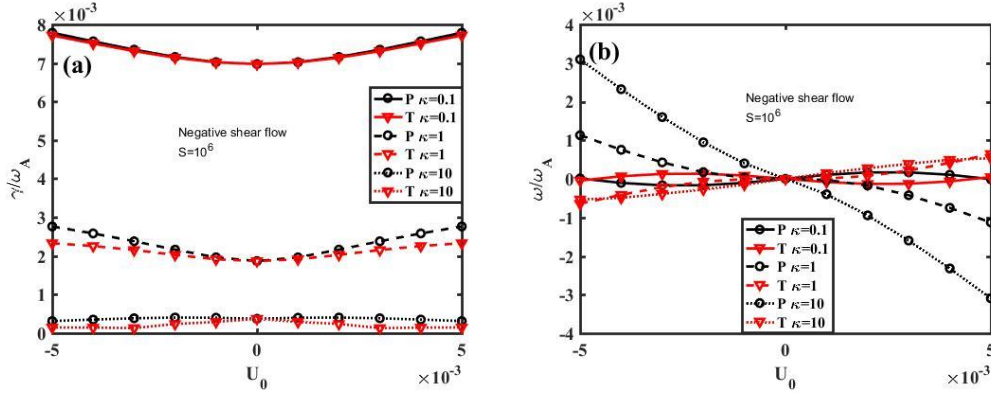


Figure 15. The MARS-F computed (a) growth rate, and (b) mode frequency, of the $n = 1$ resistive internal kink mode versus the on-axis parallel flow component U_0 , assuming poloidal projection (circles) and toroidal projection (triangles) of the parallel flow with different parallel viscous damping coefficients: $\kappa = 0.1$ (solid line), $\kappa = 1$ (dashed line) and $\kappa = 10$ (dotted line). The parallel flow is a step-wise constant with a local negative shear flow. The Lundquist number is $S = 10^6$. The 1D equilibrium toroidal flow is excluded.

5. Conclusion and discussion

We have numerically carried out a systematic investigation of the $n=1$ internal kink instability in a conventional aspect ratio tokamak plasma, in the presence of parallel equilibrium flow or its poloidal/toroidal projections. The effects of flow shear of the parallel flow component, as well as the plasma resistivity and viscosity, has also been investigated.

The MARS-F modeling shows that a pure parallel flow provides minor influence on the internal kink instability as well as the mode frequency. This is consistent with the intuitive understanding that the parallel flow mainly introduces a rotational transform along the equilibrium magnetic field line, without directly affecting the mode stability in particular when the flow is uniform. The parallel flow shear somewhat destroys the (uniform) rotational transform, but the eventual (destabilizing) effect on the internal kink is still weak. Similar findings have been reported for the resistive wall mode [25].

On the other hand, a much stronger destabilization always occurs by keeping only the poloidal or toroidal projection of the parallel flow. Note that this destabilization effect is appreciable even when the parallel flow speed is one order of magnitude smaller than that of the 1D toroidal flow. We also find that the computed mode growth rate is symmetric with respect to the parallel flow direction, whilst the mode frequency is anti-symmetric. This symmetry property is also confirmed by analytic calculations for the internal kink, as reported in Ref. [24] for the poloidal flow and in Appendix here for the toroidal flow. Comparing the computed mode frequency between the poloidal and toroidal projections, the sign is also reversed, resulting in a cancellation effect between two projections. This is another way of interpreting the weak effect of the parallel flow on the mode stability and mode frequency.

The flow shear of the parallel flow component slightly weakens destabilization of the IKM by the poloidal or toroidal projection. We emphasize that the flow shear of the parallel component does not fully reflect that of the poloidal/toroidal component. The latter is not straightforward to interpret since these flows are two-dimensional on the poloidal plane.

The plasma resistivity is found to be destabilizing to the IKM, agreeing with the previous results [4]. The plasma parallel viscosity, on the other hand, is found to be stabilizing to the IKM, independent of the parallel flow direction. This stabilization effect, with strong viscous damping, is effective in overcoming the destabilization effect introduced by the poloidal/toroidal projection of the parallel flow.

We remark that the present study is solely based on the fluid description of the IKM. Kinetic effects from plasma (thermal and energetic) particles are neglected. These effects have been shown to play significant roles in the IKM stability in the presence of 1D toroidal flow, according to non-perturbative MHD-kinetic hybrid computations [19]. The role of the kinetic effect, in combination with the plasma parallel flow or its poloidal/toroidal projection, remains a future research topic.

Acknowledgments

This work is supported by the U.S. DoE Office of Science under Contract Nos. DE-FG02–

Appendix: Analytic calculation of effect of toroidal flow on internal kink mode stability

The deviation below closely follows that from Ref. [24], where the poloidal equilibrium flow was assumed for a cylindrical plasma. The effect of the equilibrium flow on the IKM stability is determined by the inertial terms from the perturbed momentum balance equation. In what follows, we will therefore focus on examining the MHD energy perturbation associated with the plasma inertia

$$\begin{aligned}\delta I &= -\frac{1}{2} \int d\mathcal{G} \left[\rho \omega_1^2 \bar{\xi} \cdot \bar{\xi}^* + \rho \bar{g}_c \cdot \bar{\xi}^* \right] \\ &= -\frac{1}{2} \int d\mathcal{G} \left[\rho \omega_1^2 \bar{\xi} \cdot \bar{\xi}^* + \rho \omega_2 \bar{g}'_c \cdot \bar{\xi}^* \right]\end{aligned}\quad (\text{A.1})$$

where $d\mathcal{G} = r dr d\theta$, $\omega_1 = \sqrt{(\tilde{\omega} - \Omega_0)(\tilde{\omega} - \Omega_0 - \omega_{*i})}$, $\omega_2 = \tilde{\omega} - \Omega_0$, $\tilde{\omega} = \omega + i\gamma$. γ and ω denote the growth rate and real frequency of the internal kink mode, respectively. ρ is mass density of the plasma and Ω_0 the angular frequency of toroidal flow at the peaked value position. ξ is the perturbed plasma displacement, with ξ^* being the complex conjugate. Plasma toroidal flow also enters in the effective acceleration force

$$\bar{g}_c = 2\delta\bar{v} \times \bar{\Omega} - \delta\rho(\bar{V} \cdot \nabla \bar{V}) / \rho - \delta\bar{v} \cdot \nabla \bar{V} - \bar{V} \cdot \nabla \delta\bar{v}, \quad (\text{A.2})$$

where the perturbed plasma velocity and density can be written as $\delta\bar{v} = -i(\tilde{\omega} - m\Omega_0)\bar{\xi} = -i\omega_2\bar{\xi}$ and $\delta\rho = -\nabla\rho \cdot \bar{\xi}$, respectively, according to the two-fluid MHD model in the inertial layer given in Refs. [35] and [36]. We thus have

$$\begin{aligned}\bar{g}_c &= -i\omega_2 2\bar{\xi} \times \bar{\Omega} + \nabla\rho \cdot \bar{\xi}(\bar{V} \cdot \nabla \bar{V}) / \rho + i\omega_2 \bar{\xi} \cdot \nabla \bar{V} + i\omega_2 \bar{V} \cdot \nabla \bar{\xi} \\ &= \omega_2 \left[\left(\frac{d\rho}{\omega_2 \rho dr} \xi_r + \frac{d\rho}{\omega_2 \rho r d\theta} \xi_\theta \right) \Omega^2 R_0 \left(1 + \frac{r}{R_0} \cos\theta \right) \bar{e}_R + \Omega \bar{\xi} \right]. \\ &= \omega_2 \bar{g}'_c\end{aligned}\quad (\text{A.3})$$

where ξ_r and ξ_θ are the radial and poloidal components of the plasma displacement, respectively. R_0 is the effective major radius and V the toroidal equilibrium flow velocity. Note that components along the toroidal angle are neglected in the above Eq. (A.3), because their scalar products with $\bar{\xi}^*$ vanish. The term $\bar{g}'_c \cdot \bar{\xi}^*$ from Eq. (A.1) can be further reduced

to

$$\begin{aligned} & \bar{g}'_c \cdot \bar{\xi}^* \\ &= -\left(\frac{d\rho}{\omega_2 \rho dr} \xi_r + \frac{d\rho}{\omega_2 \rho r d\theta} \xi_\theta\right) \Omega^2 R_0 [\xi_r^* \cos \theta - \xi_\theta^* \sin \theta + \frac{r}{R_0} (\xi_r^* \cos^2 \theta \\ & \quad - \xi_\theta^* \cos \theta \sin \theta)] + \Omega \bar{\xi} \cdot \bar{\xi}^* \end{aligned} \quad (\text{A.4})$$

where the two-dimensional plasma equilibrium density $\rho(r, \theta)$ can be expressed via an one-dimensional quantity $\tilde{\rho}(r)$ as $\rho(r, \theta)/\tilde{\rho}(r) = \exp[\tilde{\rho}(r)\Omega^2(R^2 - R_0^2)/2P]$ according to Refs. [18] and [37]. R is the plasma major radius here, and P the equilibrium pressure. Substituting Eq. (A.4) into Eq. (A.1) and performing volume integration over the second inertial term, we have

$$\begin{aligned} & -\frac{1}{2} \int d\vartheta \rho \omega_2 \bar{g}'_c \cdot \bar{\xi}^* \\ &= -\frac{\pi \omega_2}{2} \int_0^{r_s} r dr \left[-\frac{\Omega^2 r}{\omega_2} \frac{d\tilde{\rho}}{dr} \xi_r^2 - \frac{\Omega^2 R_0^2}{\omega_2} \left(\frac{\tilde{\rho} \Omega^2 r}{kT}\right)' \xi_r^2 + \frac{\tilde{\rho} \Omega^4 R_0^2}{kT \omega_2} \xi_r^2 + 4\tilde{\rho} \Omega \xi_r^2 \right] \\ & \quad - \pi \omega_2 \int_0^{r_s} r dr \left(\frac{\tilde{\rho} \Omega^4 R_0^2}{kT \omega_2} + 2\tilde{\rho} \Omega \right) r \xi_r \frac{d\xi_r}{dr} - \pi \omega_2 \int_0^{r_s} r dr \left(\frac{\tilde{\rho} \Omega^4 R_0^2}{2kT \omega_2} + \tilde{\rho} \Omega \right) r^2 \left(\frac{d\xi_r}{dr} \right)^2 \end{aligned} \quad (\text{A.5})$$

where k is Boltzmann constant and r_s the position of the $q = 1$ surface.

Next, we assume analytic radial profiles for the plasma density $\tilde{\rho}(r)$, the plasma toroidal rotation $\Omega(r)$, and the plasma temperature $T(r)$ as

$$\tilde{\rho}(r) = \rho_0 f(r), \quad \Omega = \Omega_0 g(r), \quad T = T_0 u(r), \quad (\text{A.6a})$$

with

$$\begin{aligned} f(r) &= \rho_0 \left[1 - \left(\frac{r}{a}\right)^2\right]^{\sigma_\rho} \quad \text{and} \quad \frac{df}{dr} = -2\sigma_\rho \left[1 - \left(\frac{r}{a}\right)^2\right]^{\sigma_\rho - 1} \frac{r}{a^2}, \\ g(r) &= \Omega_0 \left[1 - \left(\frac{r - r_\Omega}{a}\right)^2\right]^{\sigma_\Omega} \quad \text{and} \quad \frac{dg}{dr} = -2\sigma_\Omega \left[1 - \left(\frac{r - r_\Omega}{a}\right)^2\right]^{\sigma_\Omega - 1} \frac{r - r_\Omega}{a^2}, \\ u(r) &= T_0 \left[1 - \left(\frac{r}{a}\right)^2\right]^{\sigma_T} \quad \text{and} \quad \frac{du}{dr} = -2\sigma_T \frac{r}{a^2} \left[1 - \left(\frac{r}{a}\right)^2\right]^{\sigma_T - 1}. \end{aligned} \quad (\text{A.6b})$$

where a is the plasma minor radius. ρ_0 and T_0 are the on-axis plasma density and temperature respectively. r_Ω is the peaked position of toroidal rotation profiles.

The plasma radial displacement ξ_r and its radial gradient $\frac{d\xi_r}{dr}$ can be approximated by the following step-like function [24]

$$\xi_r = \begin{cases} \xi_0, & r < r_s - \frac{\Delta}{2} \\ \xi_0 \left[1 - \frac{(r - r_s)}{\Delta} \right], & r_s - \frac{\Delta}{2} < r < r_s + \frac{\Delta}{2} \\ 0, & r > r_s + \frac{\Delta}{2} \end{cases}, \quad \frac{d\xi_r}{dr} = \begin{cases} 0, & r < r_s - \frac{\Delta}{2} \\ -\frac{\xi_0}{\Delta}, & r_s - \frac{\Delta}{2} < r < r_s + \frac{\Delta}{2} \\ 0, & r > r_s + \frac{\Delta}{2} \end{cases}. \quad (\text{A.7})$$

where $\Delta = \sqrt{3}R_0\omega_1/iq'_sV_A$. Carrying out analytic integration along the plasma minor radius in Eq. (A.5), we arrive at

$$\begin{aligned} & -\frac{1}{2} \int d\vartheta \rho \omega_2 \bar{g}'_c \cdot \bar{\xi}^* \\ & = -\pi \rho_0 \Omega_0 \omega_2 r_s^2 \xi_0^2 [T_1 + (T_2 + \frac{\Omega_0^2 R_0^2}{2kT_0} T_3) \frac{\Omega_0}{\omega_2} + (\frac{\Omega_0^3 R_0^2}{2kT_0 \omega_2} \frac{g_1^4}{u_1} + g_1) (\frac{i\hat{s}^2 \omega_A}{\omega_1} - 2)] f_1 \end{aligned}, \quad (\text{A.8})$$

where $\hat{s} = r_s q'_s$, $\omega_A = V_A / (\sqrt{3}R_0 r_s q'_s)$, $T_1 = \frac{2}{f_1} \int_0^1 \hat{r} d\hat{r} f(\hat{r}) g(\hat{r})$,

$T_2 = -\frac{1}{2f_1} \int_0^1 \hat{r}^2 d\hat{r} g^2(\hat{r}) \frac{df(\hat{r})}{d\hat{r}}$ and $T_3 = -\frac{1}{f_1} \int_0^1 \hat{r}^2 d\hat{r} g^2(\hat{r}) \frac{d}{d\hat{r}} \left(\frac{f(\hat{r}) g^2(\hat{r})}{u(\hat{r})} \right)$. q'_s is gradient

of the safety factor profile at the $q=1$ surface, and $\hat{r} = r/r_s$, $f_1 = f(\hat{r}=1)$,

$g_1 = g(\hat{r}=1)$, $u_1 = u(\hat{r}=1)$.

The first inertial term satisfies

$$-\frac{1}{2} \int d\vartheta \rho \omega_1^2 \bar{\xi} \cdot \bar{\xi}^* = -\frac{\pi \rho_0 \omega_1^2 \xi_0^2 r_s^3}{\Delta} f_1, \quad (\text{A.9})$$

Substituting Eqs. (A.8) and (A.9) into Eq. (A.1), the perturbed inertial term is calculated as

$$\begin{aligned} \delta I = C_0 & \left(-i \frac{\omega_1}{\omega_A} \right) \left[1 + \frac{g_1 \Omega_0}{\omega_1} - i \frac{\Omega_0}{\hat{s}^2 \omega_A} [T_1 + (T_2 + (T_3 - \frac{2g_1^4}{u_1}) \frac{\Omega_0^2 R_0^2}{2kT_0}) \frac{\Omega_0}{\omega_2} - 2g_1] \right. \\ & \left. + \frac{\Omega_0^2 R_0^2}{2kT_0} \frac{g_1^4}{u_1} \frac{\Omega_0^2}{\omega_1^2} \right] f_1 \end{aligned}, \quad (\text{A.10})$$

which is further normalized to

$$\delta \hat{I} = -i \frac{\omega_1}{\omega_A} \left[1 + \frac{g_1 \Omega_0}{\omega_1} + i \frac{\Omega_0}{\hat{s}^2 \omega_A} [C_1 + \frac{(C_2 + C_3 \Theta) \Omega_0}{\omega_2}] + \frac{\Theta g_1^4}{u_1} \frac{\Omega_0^2}{\omega_1^2} \right] f_1, \quad (\text{A.11})$$

with the normalized factor of $C_0 = \frac{1}{3} \frac{B_0^2 \xi_0^2 r_s^2}{4R_0^2}$, i.e. $\frac{\delta I}{C_0} = \delta \hat{I}$. In the above, $\Theta = \frac{m_i \Omega_0^2 R_0^2}{2kT_0}$,

$C_1 = 2g_1 - T_1$, $C_2 = -T_2$, and $C_3 = \frac{2g_1^4}{u_1} - T_3$. With the assumption of a subsonic flow, the

Θ value is small and all terms associated with Θ from Eq. (A.11) can be neglected. Consequently, Eq. (A.11) helps us to establish a dispersion relation for the IKM stability including the effects of toroidal flow

$$-i \frac{\omega_1}{\omega_A} \left[1 + \frac{g_1 \Omega_0}{\omega_1} + i \frac{\Omega_0}{\hat{s}^2 \omega_A} \left[C_1 + \frac{C_2 \Omega_0}{\omega_2} \right] \right] f_1 + \delta \hat{W}_c = 0. \quad (\text{A.12})$$

An approximate analytical solution of Eq. (A.12) is obtained as

$$\begin{aligned} \gamma &= - \left(1 + \frac{C_1^2 \Omega_0^2}{\hat{s}^4 \omega_A^2} \right)^{-1} \left(\frac{C_2 - g_1 C_1}{\hat{s}^2 \omega_A} + \frac{\omega_A \delta \hat{W}_c}{\Omega_0^2 f_1} \right) \Omega_0^2, \\ \omega &= \Omega_0 + \frac{\omega_{*i}}{2} + \left(1 + \frac{C_1^2 \Omega_0^2}{\hat{s}^4 \omega_A^2} \right)^{-1} \left(-g_1 - \frac{C_1 C_2 \Omega_0^2}{\hat{s}^4 \omega_A^2} - \frac{C_1 \delta \hat{W}_c}{\hat{s}^2 f_1} \right) \Omega_0 \end{aligned}, \quad (\text{A.13})$$

showing that the mode growth rate is symmetric with respect to the toroidal flow direction, while the mode frequency is anti-symmetric (without taking into account the diamagnetic flow correction). This analytic solution thus qualitatively verifies the symmetry properties for the MARS-F computed IKM eigenvalues as reported in Fig. 10(e-f).

We also note that Eqs. (A.12) and (A.13) have similar form to that reported in Ref. 24 with poloidal equilibrium flow. In fact, the mathematical form of the eigenvalue solutions can be made identical between two types of flows, by switching the reference direction of the toroidal flow (i.e. switching the sign of the above g -factor) and by re-defining the C_1 and C_2 factors in Ref. 24. This explains why the effects of toroidal and poloidal flows on the internal kink mode are similar, as found in MARS-F computations reported in this work.

References

- [1] Chen L., White R.B., Rosenbluth M.N. 1984 Phys. Rev. Lett. **52** 1122-1125
- [2] Coppi B., Porcelli F. 1986 Phys. Rev. Lett. **57** 2272-2275
- [3] Coppi B., Detragiache P., Migliuolo S., Pegoraro F., Porcelli F. 1989 Phys. Rev. Lett. **63** 2733
- [4] Wu T., He H., Liu Y., Liu Y., Hao G.Z., Zhu J. 2018 Phys. Plasmas **25** 052504
- [5] Miao Y. *et al*/2020 Nucl. Fusion **60** 096022
- [6] Goeler S.v., Stodiek W., Sauthoff N. 1974 Phys. Rev. Lett. **33** 1201
- [7] White R.B., Rutherford P.H., Colestock P., Bussac M.N. 1988 Phys. Rev. Lett. **60** 2038-2041
- [8] Porcelli F., Bouche D., Rosenbluth M.N. 1996 Plasma Phys. Control. Fusion **38** 2163-2186
- [9] Zhou L., Liu Y., Siccino M., Fable E., Wu T., Duan P., Chen L. 2020 Nucl. Fusion **60** 126011

- [10] McGuire K. *et al*/1983 Phys. Rev. Lett. **50** 891-895
- [11] Sauter O. *et al*/2002 Phys. Rev. Lett. **88** 105001
- [12] Furukawa M., Tokuda S. 2005 Nucl. Fusion **45** 377-383
- [13] Waelbroeck F.L. 1996 Phys. Plasmas **3** 1047
- [14] Wahlberg C. 2005 Plasma Phys. Control. Fusion **47** 757-775
- [15] Wahlberg C., Bondeson A. 2001 Physics of Plasma **8** 3595
- [16] Bondeson A., Ward D.J. 1994 Phys. Rev. Lett. **72** 2709-2712
- [17] Xia G., Liu Y., Liu Y. 2014 Plasma Phys. Control. Fusion **56** 095009
- [18] Wahlberg C., Bondeson A. 2000 Phys. Plasmas **7** 923
- [19] Wu T., Liu Y., Liu Y., Zhou L., Hongda H. 2019 Physics of Plasma **26** 102102
- [20] Cromb  K. *et al*/2005 Phys. Rev. Lett. **95** 155003
- [21] Tala T. *et al*/2007 Nucl. Fusion **47** 1012-1023
- [22] Ida K., Fujita T. 2018 Plasma Phys. Control. Fusion **60** 033001
- [23] Mendonca J., Chandra D., Sen A., Thyagaraja A. 2018 Phys. Plasmas **25**, 022504
- [24] Xie W. 2020 Phys. Plasmas **27** 092504
- [25] Xia G., Liu Y., Li L., Ham C.J., Wang Z.R., Wang S. 2019 Nucl. Fusion **59** 126035
- [26] Chen X.L., Morrison P.J. 1990 Phys. Fluids B **2** 2575
- [27] Ofman L., Chen X.L., Morrison P.J. 1991 Phys. Plasmas **3** 1364
- [28] Ren C., Chu M.S., Callen J.D. 1999 Phys. Plasmas **5** 1203
- [29] Takeda K., Agullo O., Benkadda S., Sen A., Bian N., X. G. 2008 Phys. Plasmas **15** 022502
- [30] Haye R.J.L., Buttery R.J. 2009 Phys. Plasmas **16** 022107
- [31] Wang S., Ma Z.W. 2015 Phys. Plasmas **22** 122504
- [32] Chu M.S., Greene J.M., Jensen T.H., Miller R.L., Bondeson A., Johnson R.W., Mauel M.E. 1995 Phys. Plasmas **2** 2236-2241
- [33] Liu Y.Q., Bondeson A., Fransson C.M., Lennartson B., Breitholtz C. 2000 Phys. Plasmas **7** 3681-3690
- [34] L tjens H., Bondeson A., Sauter O. 1996 Comput. Phys. Commun. **97** 219-260
- [35] Fogaccia G., Romanelli F. 1995 Phys. Plasmas **2** 227
- [36] Shi B., Sui G. 1997 Phys. Plasmas **4** 2785
- [37] Wahlberg C., Chapman I.T., Graves J.P. 2009 Phys. Plasmas **16** 112512